Characterization of One-Dimensional Capacitive Micromachined Ultrasonic Immersion Transducer Arrays

Xuecheng Jin, *Student Member, IEEE*, Ömer Oralkan, *Student Member, IEEE*, F. Levent Degertekin, *Member, IEEE*, and Butrus T. Khuri-Yakub, *Fellow, IEEE*

***Abstract*—In this paper, we report on the characterization of 1-D arrays of capacitive micromachined ultrasonic transducers (cMUT). A 275- × 5600-μm 1-D CMUT array element is experimentally characterized, and the results are found to be in agreement with theoretical predictions. As a receiver, the transducer has a 0.28-fm/$\sqrt{Hz}$ displacement sensitivity, and, as a transmitter, it produces 5 kPa/V of output pressure at the transducer surface at 3 MHz with a DC bias of 35 V. The transducer has more than 100% fractional bandwidth around 3 MHz, which makes it suitable for ultrasound imaging. The radiation pattern of isolated single elements, as well as those of array elements are measured, and two major sources of acoustical cross talk are identified. A weakly dispersive non-leaky interface wave (Stoneley wave) is observed to be propagating at the silicon substrate-fluid interface at a speed close to the speed of sound in the fluid. This wave causes internal reflections, spurious resonance, and radiation from the edges of the silicon substrate. The large lateral component of the particle velocity generated by the membranes at the edge of the cMUT array elements is found to be the source of this interface wave. Lowest order Lamb waves in the silicon substrate are also found to contribute to the cross talk between elements. These waves are excited at the edges of individual vibrating membranes, where they are anchored to the substrate, and result in a narrowing of the beam profile of the array elements. Several methods, such as trench isolation and wafer thinning, are proposed and implemented to modify the acoustical cross coupling between array elements.**

I. Introduction

CMUTs are an attractive alternative to conventional piezoelectric transducers [1]. They offer the advantage of increased bandwidth with comparable sensitivity to piezoelectric transducers as well as ease of fabrication and electronics integration [2]. The fabrication process and theoretical modeling of single cMUT devices were reported earlier [2]–[4]. Many applications, especially immersion imaging applications, demand better understanding and improvement of cMUTs both in terms of individual device performance and array behavior. Cross coupling between elements is one of the most important factors affecting the performance of an imaging array [5]. The level of these disturbances can be quantified by radiation pattern measurements, electrical measurements, and by detection of structural displacements using optical probes [6].

The aim of this paper is to characterize the performance of the 1-D cMUT arrays and identify and suggest solutions to the acoustical cross talk problems. Several 1-D cMUT arrays as well as test structures consisting of single isolated elements have been fabricated for this purpose. In this paper, the electrical equivalent circuit of a cMUT is briefly explained for completeness. The results of transmit and receive experiments are presented and compared with theoretical calculations in detail. Radiation pattern and optical probe measurements are performed to investigate the sources of acoustical cross talk in these array structures. Lamb waves propagating in the silicon wafer and Stoneley-type waves propagating at the fluid-silicon wafer interface are observed, and good agreement is obtained with theoretical predictions. The excitation mechanism of these spurious modes is discussed, and several methods to reduce cross coupling are suggested and implemented.

Manuscript received April 27, 2000; accepted October 13, 2000. This work was supported by grants from the U.S. Office of Naval Research, Defense Advanced Research Projects Agency, National Science Foundation, and a fellowship from the National University of Singapore.

X. Jin, Ö. Oralkan, and B. T. Khuri-Yakub are with Edward L. Ginzton Laboratory, Stanford University, Stanford, CA 94305-4085 (e-mail: xcjin@alumni.stanford.org).

F. L. Degertekin is with G. W. Woodruff School of Mechanical Engineering, Georgia Institute of Technology, Atlanta, GA 30332.

II. Electrical Equivalent Circuit

The electrical equivalent circuit model is the theoretical foundation for the design and optimization of cMUTs. A cMUT cell consists of a metalized membrane (top electrode) suspended above a heavily doped silicon substrate (bottom electrode) as shown in Fig. 1. There are many cells in a transducer element, and the elements are used to make cMUT arrays. The operation of the cMUT can be explained as follows. A DC voltage is placed between the metalized membrane and the substrate. The membrane is attracted toward the bulk, and stress within the membrane resists the attraction. The membrane is set into vibration to generate an ultrasonic wave by the application of an AC voltage to the electrode. Reversely, an AC current is induced in the electrode if an ultrasound wave impinges on the membrane.

The small signal equivalent circuit of a cMUT is a two-port network as shown in Fig. 2. This circuit was derived

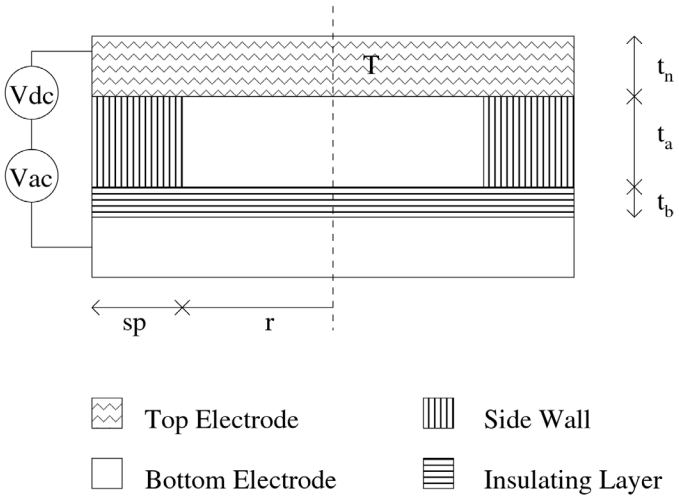

Fig. 1. The cross-section of a cMUT cell.

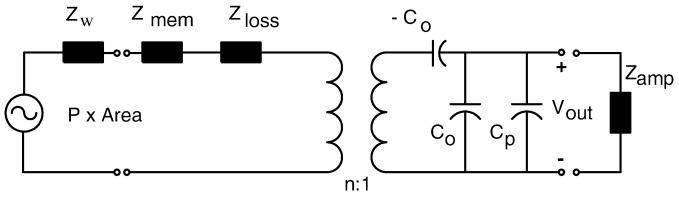

Fig. 2. Electrical equivalent circuit of a cMUT.

by Mason [7] and further developed for cMUTs [2]. In this equivalent circuit, Z_w corresponds to the mechanical impedance of water, Z_{mem} is the mechanical impedance of the membrane, and Z_{loss} accounts for the total loss. The ideal transformer in the circuit transforms velocity, a mechanical quantity, into electrical current, and C_p represents the parasitic capacitance. The value of Z_{loss} can be obtained experimentally by measuring the electrical input impedance of the cMUT in vacuum conditions, assuming that structural loss is a purely real term and not a function of the ambient pressure.

For an immersion transducer, the mechanical impedance of the water is much higher than the mechanical impedance of the membrane, which can then be ignored in the equivalent circuit. Thus, the resonant behavior that dominates the operation of piezoelectric transducers does not exist in immersion cMUTs. This inherently implies a broadband operation.

III. Single Transducer Element Characterization

Both an isolated single cMUT element and an element in a 1-D cMUT array, each with 1280 cells connected in parallel, were characterized by measuring their electrical input impedance, bandwidth, open circuit receive sensitivity, output pressure, output SNR, and radiation pattern. The physical parameters of the cMUT element are listed in Table I. The active area is 59% of the total 275- × 5600-μm element area. A dummy neighbor cMUT is located at 5 mm away from the isolated single cMUT element for cross talk testing purpose. Fig. 3 shows the top views of two 64-element 1-D cMUT arrays (a), one isolated single cMUT element with a dummy neighbor (b), and the zoom-in view of the cMUT element with 8×160 cells connected in parallel (c).

TABLE I
Physical Parameters of the cMUT.

r	Cell radius	15 μm
t_n	Membrane thickness	0.3 μm
t_a	Air-gap thickness	0.15 μm
t_b	Insulating layer thickness	0.15 μm
N	Number of cells in the element	1280

The experimental setups used for receive and transmit mode characterization are identical to the one described in [8], and the devices were manufactured using the fabrication process explained in [9].

A. Isolated Single Element

The electrical input impedance of an immersion transducer has no resonance as expected from an *RC* circuit. This is seen in Fig. 4, where the measured and calculated electrical impedance components are plotted. The value of the parasitic capacitance (C_p) is calculated as 37.9 pF for this device. This parasitic capacitance is 1.7 times larger than the device capacitance (C_0), which is 22.3 pF. Using the calculated C_p value, a good match is obtained between the measured and simulated electrical input impedance at a DC bias of 20 V as shown in Fig. 4. With this type of input impedance, the center frequency and bandwidth of the transducer are determined by the termination at the electrical port.

The same transducer was used for transmit and receive characterization in a tank filled with vegetable oil. In the receive experiment, a commercial piezoelectric transducer (Panametrics V109) was used as the transmitter. The pressure output of the piezoelectric transmitter was measured using a calibrated hydrophone at a distance of 7.5 cm. The cMUT was placed at the same location as the hydrophone. The output of the cMUT was amplified with a preamplifier with a 32-dB mid-band gain and a 3-dB bandwidth of 3.5 MHz centered at 2.5 MHz.

The measured impulse response and corresponding frequency spectrum obtained from the single isolated cMUT are shown in Fig. 5. This frequency response is limited by the transmitter and amplifier responses, and not the transducer's response. The measured output SNR is 45 dB/Pa/Hz at 3 MHz. The output noise floor of the transducer-amplifier system is measured with no input applied to the transducer. The noise floor measured at the output of the amplifier sets the limit for the minimum detectable signal for the overall system. This measured output noise floor is translated into pressure values at the input of the transducer to calculate the SNR and the min-

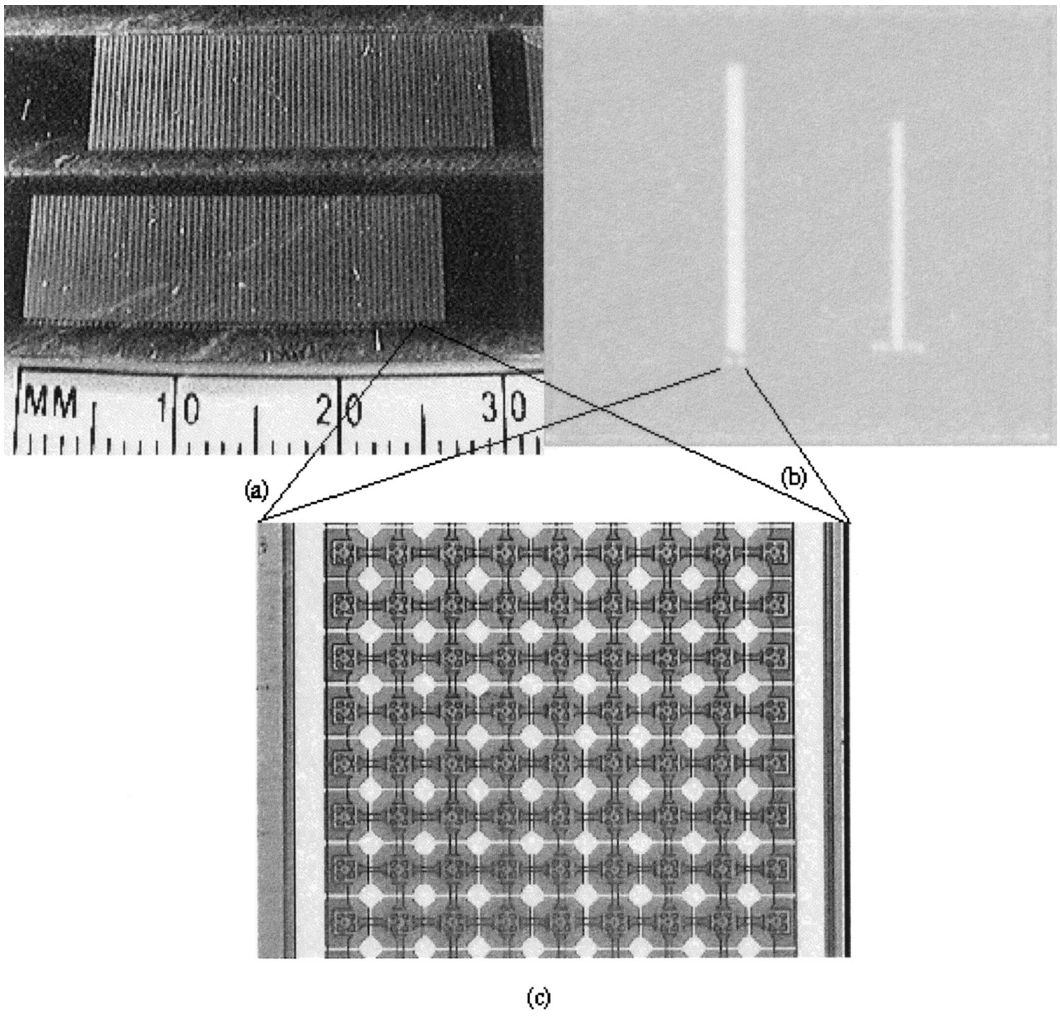

Fig. 3. Device-top views. a) Two 64-element, 1-D cMUT arrays, b) one isolated single cMUT element with a dummy neighbor, and c) zoom-in view of cMUT element with 8 x 160 cells connected in parallel.

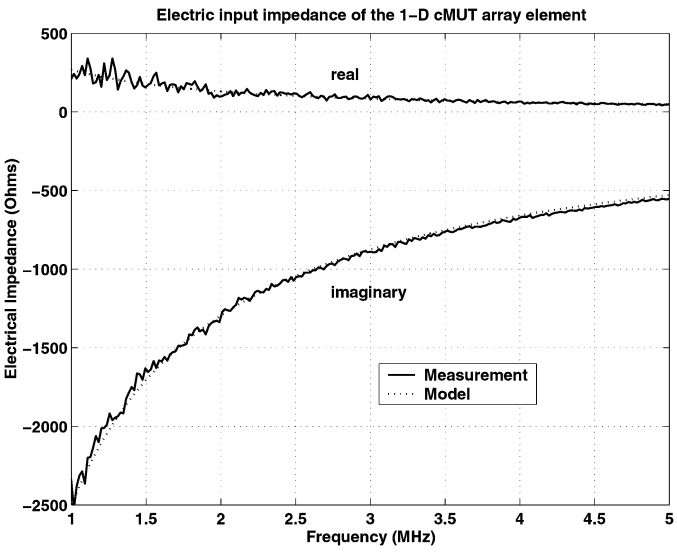

Fig. 4. Electrical input impedance of 1-D cMUT array element.

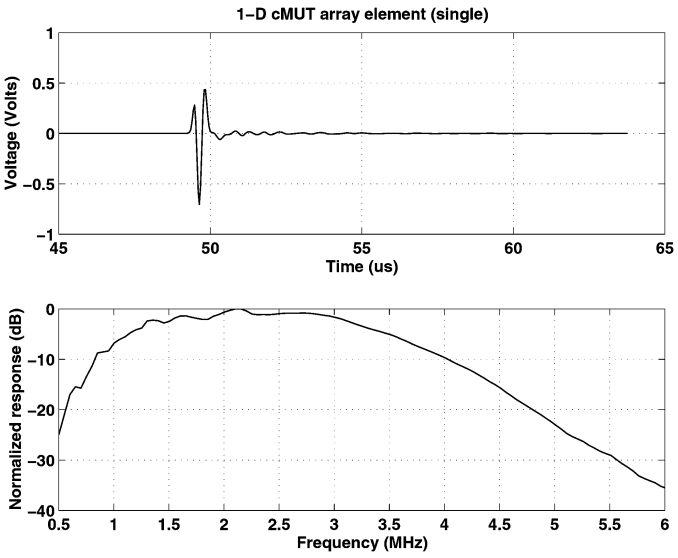

Fig. 5. Impulse and frequency responses of single device cMUT.

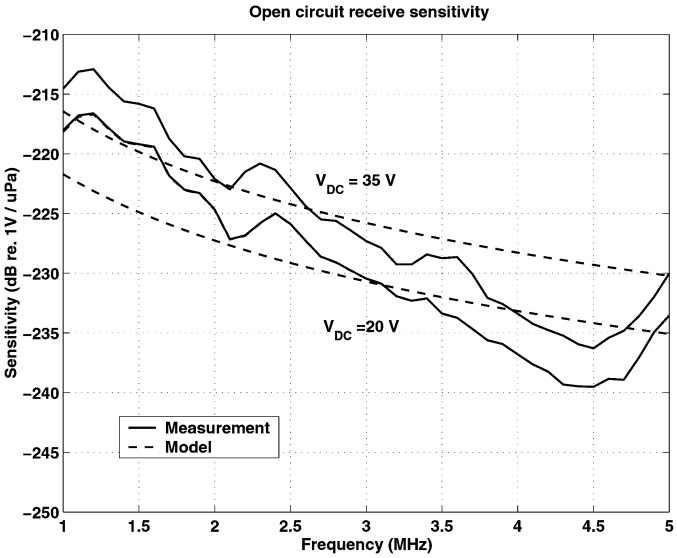

Fig. 6. Open circuit sensitivity of 1-D cMUT element.

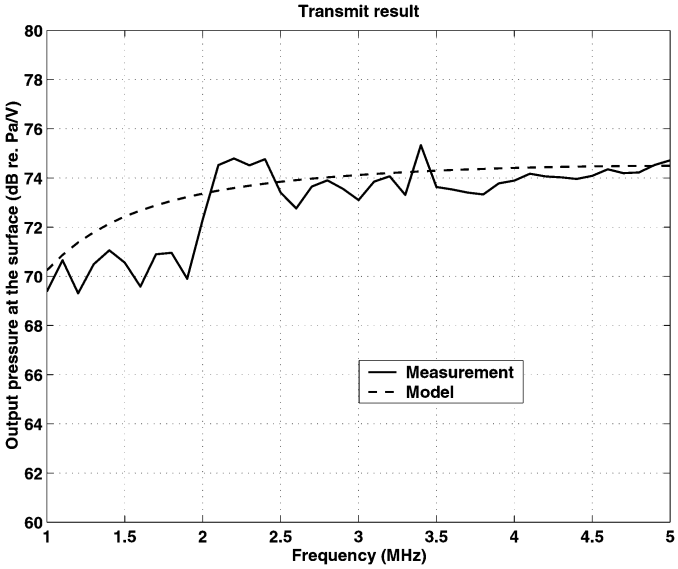

Fig. 7. Output pressure produced by the cMUT on its surface.

imum detectable pressure for the overall system. The minimum detectable pressure of the system is 7.8 mPa/$\sqrt{Hz}$, corresponding to a displacement of 0.28 fm/$\sqrt{Hz}$.

The measured and simulated open circuit receive sensitivity (OCRS) figures are shown in Fig. 6 for DC bias voltages of 20 and 35 V. The measured OCRS is -227 dB re. 1 V/μPa at 3 MHz for a DC bias voltage of 35 V. The equivalent circuit model does not model the effects of the lateral coupling of acoustical energy, which will be addressed in the following sections of this paper. Because of these effects, the difference between simulations and the measurements can be as large as 7 dB at some frequencies. However, for most frequencies the measurements are within 3 dB of the simulation results.

The pressure produced by the cMUT in transmit was measured using a calibrated hydrophone. The pressure at the cMUT surface is calculated by taking the diffraction loss into account. The measured and simulated output pressure figures at the transducer surface are shown in Fig. 7. The wide bandwidth of the cMUT is clearly observed from the flat pressure response from 1 to 5 MHz. In the simulations, the medium is modeled as a load with complex impedance. The cMUT produces 5 kPa/V of output pressure on its surface at 3 MHz, corresponding to 1.8 Å/V displacement at a DC bias of 35 V.

A dynamic range for the transducer is defined as the ratio of the pressure output at the face of the transducer to the minimum detectable pressure. The cMUT used in this work achieved a total dynamic range of 120 dB/Hz for 1 V of input voltage at a 3-MHz frequency and a DC bias of 35 V. The measured and simulated dynamic ranges are shown in Fig. 8. The equivalent circuit model is combined with the complete SPICE model of the amplifier, and the complete system is simulated in HSPICE to obtain the theoretical SNR value. This SNR value is used to calculate the theoretical dynamic range. The model used for SNR simulations does not include the lateral coupling

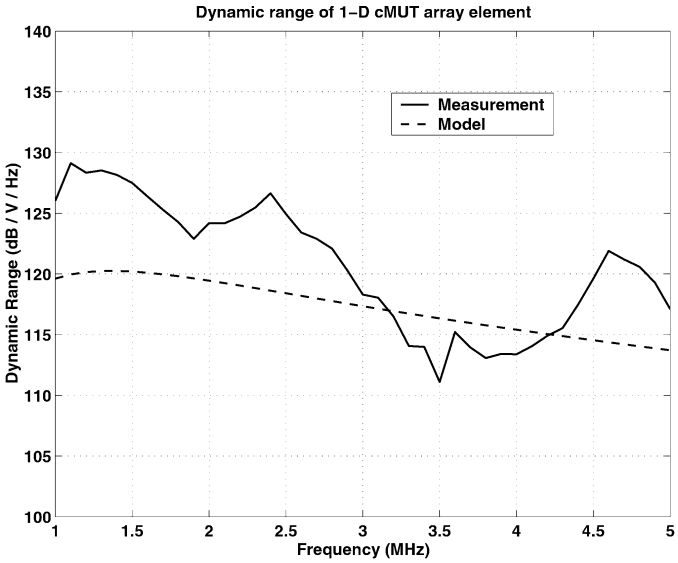

Fig. 8. Dynamic range of the transmit-receive system.

effect as explained previously. These effects are the major culprit for the differences between the simulations and the experiments. However, the experimental results have the same trend with the simulations, and the agreement is within 3 dB for most frequencies.

The radiation pattern of a cMUT element was measured using an experimental setup similar to single device characterization, except that the transmitter was allowed to rotate around its vertical axis. The receiver cMUT is fixed at a distance of 9.4 cm away from the transmitter. The transmitted signal is recorded as a function of the rotation angle when the transmitter is excited by a 100-ns square pulse with a peak voltage of 10 V.

Fig. 9 shows the time domain angular response of a single device indicating three major spurious pulses as white lines with angle-dependent time delays arriving after the

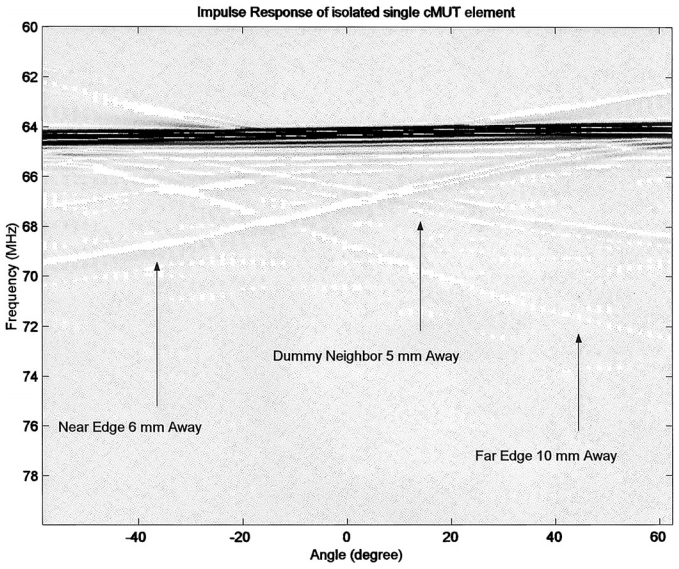

Fig. 9. Time domain angular response of the single device cMUT.

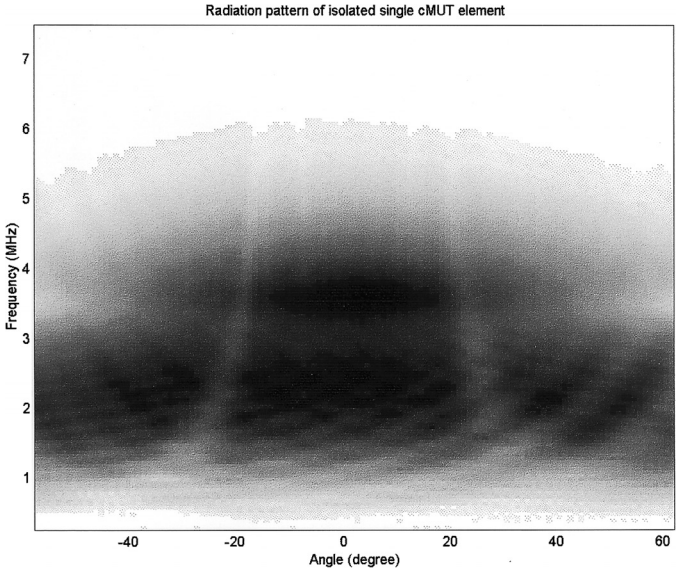

Fig. 10. Frequency domain angular response of the single device cMUT.

main pulse. Please note that there is a dummy element on the same substrate, with unconnected floating electrical terminals, which is located 5 mm away from the transmitting element. The Stoneley-type interface waves travel along the fluid-silicon substrate interface after the excitation of the transmitting cMUT element. One of the spurious pulses results from the excitation of the dummy element by the interface wave. The other two spurious pulses are due to the reflection of the interface waves and their mode conversion at the two edges of the silicon substrate, which are 6 and 10 mm away from the active element. In the same figure, one can also observe pulses arriving before the main pulse, especially for angles greater than 20°. These indicate that there is a spurious mode in the wafer with a group velocity around 4500 m/s. This corresponds to the A0 mode Lamb wave in 0.5-mm thick silicon plate in the 1- to 3-MHz range. The frequency domain angular response was obtained by taking the Fourier transform of the time domain angular response as shown in Fig. 10. The significant features of the frequency domain angular response of a single device cMUT are the dispersion curve of the A0 mode leaky Lamb wave, which has a critical angle of 38° at 1 MHz and converges to around 20° at higher frequencies. The effect of the S0 mode Lamb wave is seen at higher frequencies at an angle of 12°. The periodic ripples, especially below 3.5 MHz, are due to the spurious echoes from the edges and the excitation of the dummy element. The observed spurious effects from the Stoneley-type waves and Lamb waves will be further discussed in detail in the cross talk analysis sections.

B. Array Transducer Element

As compared with isolated single cMUT element device, cross coupling effects are more observable for 1-D array cMUT elements.

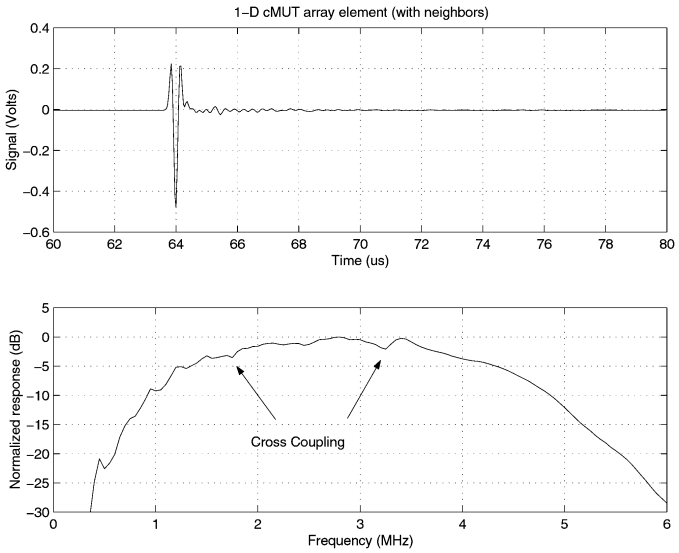

Fig. 11. Impulse and frequency responses of the 1-D cMUT array element.

The impulse response of a 1-D array element and its frequency spectrum are shown in Fig. 11. It is observed that the array element has a longer ring down time than the single device (Fig. 5). In addition, effects of cross coupling is observed around 1.8 and 3.4 MHz in the frequency domain response.

When the time domain impulse response is displayed as a function of angle, the effect of cross coupling is more evident. As shown in Fig. 12, the time domain angular response of the array element shows additional acoustic radiation from each of the neighboring elements. These additional cycles resulting from the neighboring elements are 24 dB below the main pulse and show up as a dispersive curve in the frequency spectrum shown in Fig. 13. Also, the interface waves reflected from the neighbors of

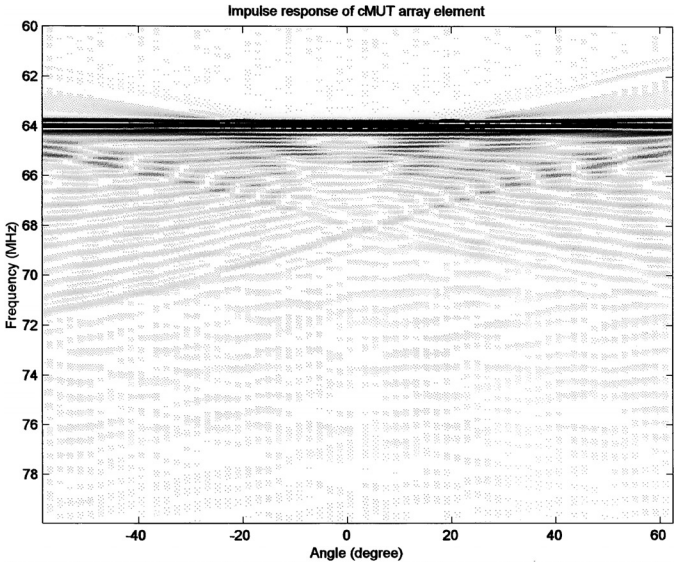

Fig. 12. Time domain angular response of the array element cMUT.

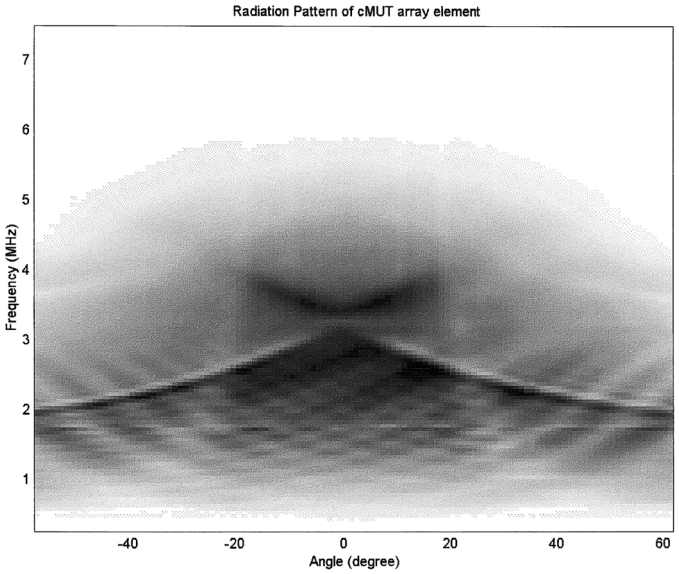

Fig. 13. Frequency domain angular response of the array element cMUT.

the transmitting element result in a resonance at a frequency of around 1.8 MHz, where the periodicity is twice the pitch of the array elements (400 μm). This strong resonance around 1.8 MHz is seen as a narrow non-dispersive horizontal line in Fig. 13.

IV. Acoustical Cross Coupling Analysis

To find ways to reduce the undesired effects of acoustical cross talk, the sources of the problems have to be identified. Preliminary results on this research were published elsewhere [10]. The basic physical structure of an immersion cMUT is a solid silicon plate with fluid on both sides or with fluid on one side and a solid integrated circuit silicon plate bonded on the other side. These boundary conditions associated with cMUTs provide the environment for the excitation and propagation of the various spurious modes such as Lamb waves, Stoneley wave, etc. In the following, each of these major cross coupling sources is discussed, and the results of their identification and reduction efforts are reported.

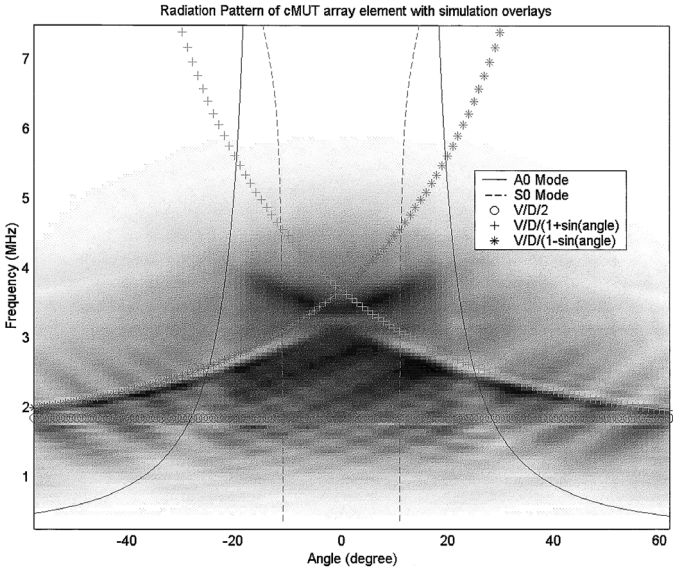

Fig. 14. Radiation pattern of cMUT array element with simulation overlays.

A. Lamb Wave Cross Coupling

Lamb waves refer to the elastic modes of propagation in a solid plate with free boundaries. The displacement of Lamb waves has components both in the direction of wave propagation and in the direction perpendicular to the plane of the plate. Lamb waves are classified into two categories; each has zero, first, second, and higher order modes. Symmetric Lamb waves have the displacement symmetrical with respect to the center plane of the plate, but anti-symmetric Lamb waves have the displacement anti-symmetrical with respect to the center plane of the plate [11]. When the Lamb wave propagates in the fluid-loaded silicon substrate, it will suffer leakage into the fluid at a radiation angle dictated by Snell's law. Because of the dispersive nature of the Lamb waves, the radiation pattern of the micromachined immersion transducer array will be a strong function of the plate thickness and frequency of operation.

One can calculate the critical angles of Lamb wave modes of this plate in a given fluid using well-known techniques and compare with the experimental radiation pattern [11]–[13]. Fig. 14 shows the calculated variation of A0 and S0 mode Lamb wave critical angles as a function of frequency [14] superimposed on the measured radiation pattern. The calculation is done only for the A0 and S0 mode Lamb waves because only these two modes propagate in the given frequency range. The simulation results

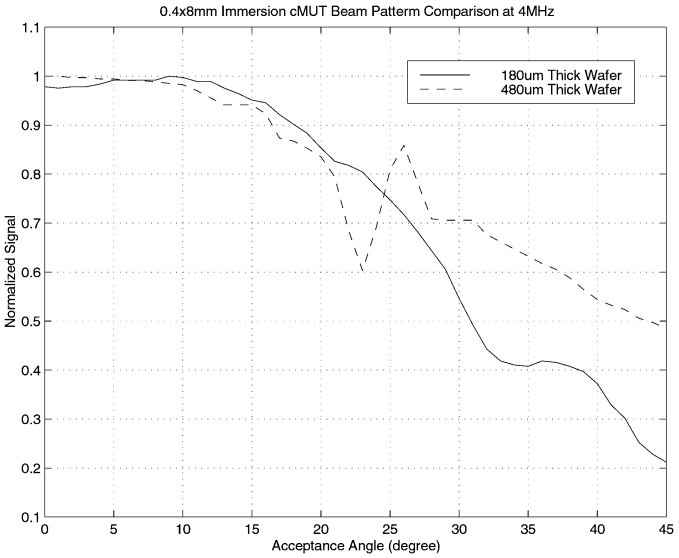

Fig. 15. Radiation pattern of cMUT for different substrate thickness with operating frequency of 4 MHz.

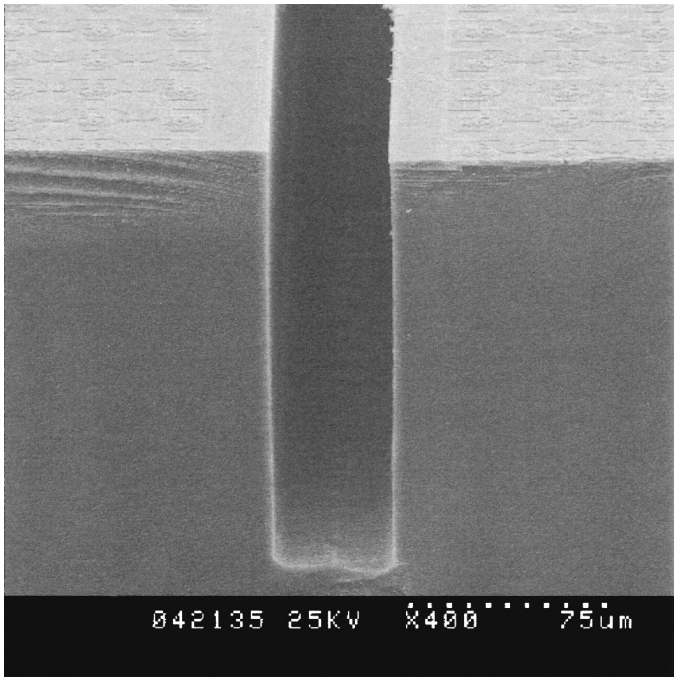

Fig. 16. Deep trench isolation between cMUT array elements.

are in agreement with the measurements. Also note the dominance of the A0 mode in the radiation pattern as compared with the S0 mode, especially at lower frequencies. This is due to the fact that the A0 mode particle velocity vector is mostly out of the plane; hence, this mode radiates efficiently into the fluid medium. In contrast, the S0 mode particle velocity is mostly in plane, especially at lower frequencies, resulting in much smaller radiation. These wave modes are excited by the stresses applied on the silicon surface at the edges where the cMUT membranes are anchored to the surface. This excitation scheme also favors the A0 mode as discussed elsewhere [15].

One can take advantage of the dispersion characteristic of the Lamb waves to modify the radiation pattern of the cMUT. For example, we move the critical angle of the A0 mode outside the acceptance angle of interest by decreasing the thickness of the silicon wafer. An experiment compares the radiation patterns of cMUTs with plate thickness of 480 and 180 μm as shown in Fig. 15. The A0 mode Lamb wave radiation angle has now moved from 22° to 35°.

Because Lamb wave propagation carries the coupled energy from other elements through the silicon bulk, reducing the effective bulk depth of the propagation path helps to reduce the cross coupling. This is verified by etching a 55-μm wide and 200-μm deep trench into the silicon substrate between neighboring elements (400 μm pitch) by deep reactive ion etching [16] as shown in Fig. 16. Comparing the angular frequency response of cMUTs with and without trench isolation as shown in Fig. 13 and Fig. 17, we conclude that deep trench isolation results in a significant improvement in cross coupling caused by Lamb waves. It is seen that the cross coupling caused by A0 and S0 mode Lamb waves is greatly suppressed, especially in the 2- to 4.5-MHz range.

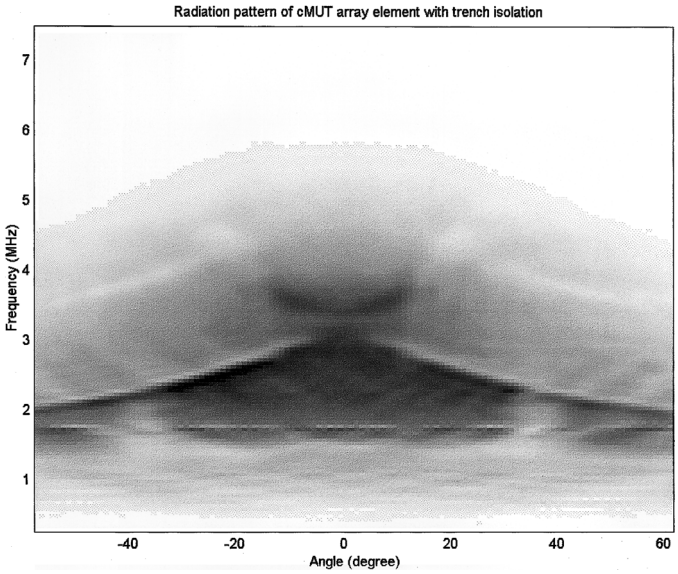

Fig. 17. Frequency domain radiation pattern with trench isolation.

B. Stoneley Wave Cross Coupling

At the plane interface between an ideal fluid and an elastic solid, two kinds of surface waves can propagate [17]. One is the so-called leaky Rayleigh wave; the other is a particular case of a Stoneley wave. A Stoneley-type wave can also propagate at the plane interface formed between a semi-infinite fluid and the top or bottom surface of a solid plate with finite thickness. With the required conditions of continuity at the interface, it is found that the Stoneley wave is composed of evanescent plane wave components in all of the media involved [18]. All of these waves have the

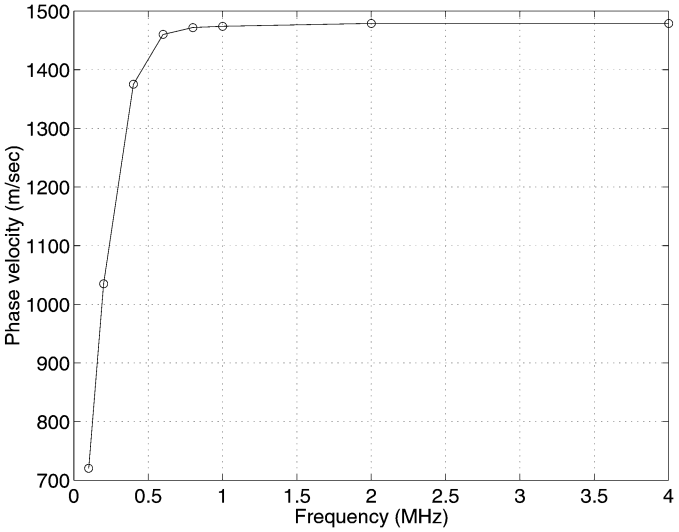

Fig. 18. Calculated Stoneley wave phase velocity.

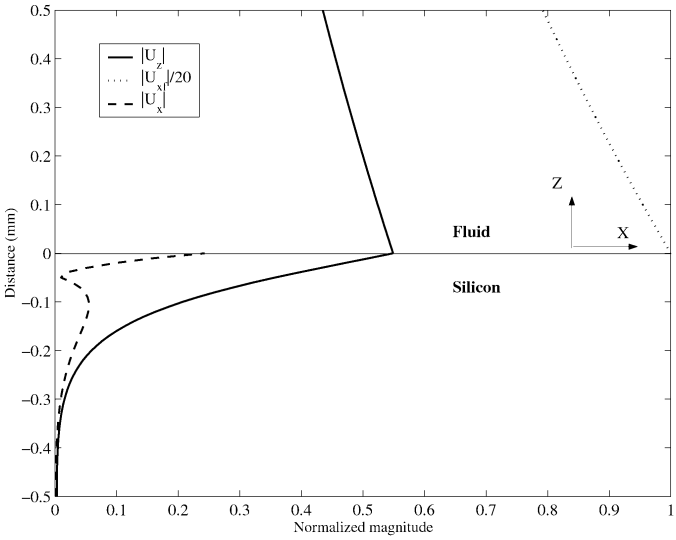

Fig. 19. Calculated Stoneley wave displacement field distribution at 4 MHz. U_x and U_{xf} are the lateral components in silicon and fluid, respectively. U_z denotes the normal particle displacement component, which is continuous at the interface.

same projection of their wave vector on the interface, and, thus, their combination gives the Stoneley wave. This undamped, nearly non-dispersive propagating Stoneley wave along the solid-liquid interface can cause significant cross coupling. In practice, the cMUT arrays will be bonded either to another wafer carrying signal processing electronics as discussed in [16], which will result in an air backing, or they will be bonded to a solid substrate. In either case, Stoneley waves can travel along the front surface of the cMUT arrays. Assuming that the air-backed cMUT can be modeled as an infinite fluid/silicon plate/vacuum structure, one can calculate the phase velocity dispersion curve and the acoustic field distributions of the Stoneley wave. In Fig. 18, the variation of the Stoneley wave phase velocity is plotted as a function of frequency for a 500-μm thick silicon plate loaded with oil on one surface. The speed of sound in the oil is taken as 1480 m/s, and the density is 980 kg/m^3. As expected, the phase velocity is nearly non-dispersive after 1 MHz, where it reaches a value of 1470 m/s. Further information on the Stoneley wave characteristics can be obtained by plotting the field distributions. The magnitude of the lateral (U_x) and vertical (U_z) displacement field components at the frequency of 4 MHz is plotted as a function of depth in Fig. 19, which shows the evanescent nature of the wave components both in silicon and the fluid. Even at this frequency, the displacement field in the silicon plate decays rapidly, indicating that the wave cannot sense the difference between a finite thickness plate or a half space. This is also reflected in the non-dispersive behavior at higher frequencies in Fig. 18. Also note that the lateral component of the particle velocity in the fluid is scaled down by 20 times to fit all of the components in the same curve. Hence, most of the energy of the Stoneley wave is carried in the fluid at the vicinity of the surface. This leads one to conclude that the large lateral fluid displacement induced at the edge of the vibrating cMUT membrane and the displacement on the silicon surface caused by the anchoring edges match the mode shape of the Stoneley wave and act as an efficient source for this wave mode.

The direct propagation of the Stoneley wave and its reflection and mode conversion at the edge of the silicon substrate contribute to the cross talk between elements. The direct and reflected Stoneley waves set any membrane along its path into motion. These membranes will radiate energy into the fluid, which is detected as cross coupling between elements. Radiation from the mode-converted Lamb waves will also contribute to the cross talk between elements.

An optical displacement probe was used to measure the displacement of the surface of the silicon wafer at 1.4 and 2.4 mm away from an isolated 1-D array element excited by a 10-ns square pulse with a peak voltage of 10 V. Fig. 20 shows that the measured signals at these two points are essentially the same, except for a time delay of 0.7 μs, which corresponds to a non-dispersive phase velocity of 1470 m/s. The displacement at the first point is propagated using the phase velocity dispersion curve of the Stoneley wave, and the result is in excellent agreement with the measured displacement at the second point [19]. This is consistent with the fact that the acoustic pulse has frequency components in the 1- to 9-MHz range.

In the frequency domain angular response of the cMUT array element as shown in Fig. 13, the major effects of the cross coupling are the horizontal and diagonal traces. These traces can be verified by theoretical simulation of Stoneley wave propagation at the solid-liquid interface with phase velocity of 1470 m/s and geometrical considerations. In the cMUT array radiation pattern measurement, the transmitter array element pitch, D, is 400 μm, and the fixed receiver is at a distance of 9 cm. The cross coupling traces that start at 2 MHz, around 60°, and form an arc to reach 3.4 MHz, around 0°, are due to the geomet-

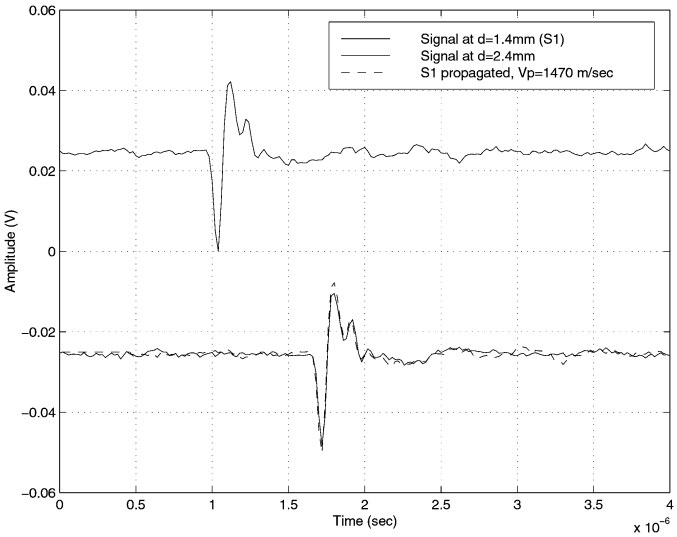

Fig. 20. Optical displacement signals caused by Stoneley wave.

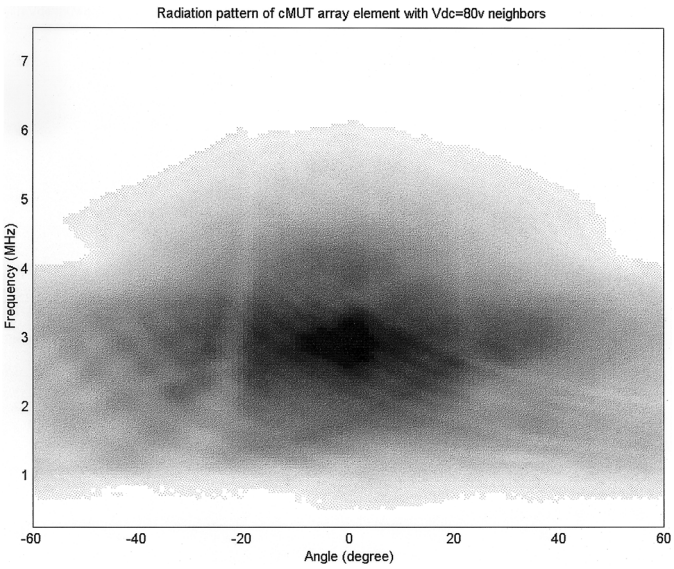

Fig. 21. Radiation pattern with higher DC bias for neighboring elements.

ric effects. When the transmitter is rotated at an angle of θ, the additional travel distance between neighboring elements is either $D + Dsin(\theta)$ or $D - Dsin(\theta)$ for rotation away or toward the receiver. So the excitation of one element will cause delayed transmission from neighboring elements by Stoneley wave cross coupling. The frequency domain representation of this periodic distance change is either $V/D(1+sin(\theta))$ or $V/D(1-sin(\theta))$ as shown in the frequency domain angular response plots along with their second harmonics.

The frequency domain cross coupling patterns are shown as overlays in Fig. 14, which agree very well with the radiation pattern measurements superimposed upon. The disagreement at higher frequencies can be due to the fact that the structure at the silicon surface begins to affect the Stoneley wave velocity, because the fields get concentrated predominantly at the fluid-transducer surface interface at higher frequencies. This fine structure is obviously not taken into account in the calculations.

The effect of traveling Stoneley waves on the impulse response is verified by electrically changing the acoustic properties of the cMUT membrane. When a DC bias that exceeds the collapse voltage is applied to neighboring elements, their membrane motion is significantly suppressed. Thus, the delayed transmissions from the neighboring elements are prevented. Comparing the radiation pattern in Fig. 13 (with normal DC bias for neighboring elements) and that in Fig. 21 (with high DC bias for neighboring elements), it is evident that the effect of the Stoneley wave cross coupling on the impulse response is significantly reduced.

To reduce Stoneley wave cross coupling between neighboring elements, the boundary conditions of the cMUT surface can be modified to prevent efficient Stoneley wave excitation and propagation. The excitation can be reduced by decreasing the slope of the vertical displacement at the edge of the cMUT. Alternately, a lossy medium can be placed between neighboring elements or altering the orientation of neighboring elements. In addition, a lossy material can by placed at the edges of cMUT device to prevent Stoneley wave mode conversion and transmission along the edges. Fig. 22 shows the angular impulse responses of the same isolated single cMUT element with a dummy neighbor with silicon-soft, epoxy-liquid edge, where UV curable epoxy was applied to the original wafer edge and partially cured on the surface, leaving soft epoxy inside uncured. Compared with the normal silicon-liquid edge impulse response as shown in Fig. 12, it is clear that the two cross coupling traces from the device edges are reduced significantly because of the absorption of the Stoneley waves by the lossy epoxy.

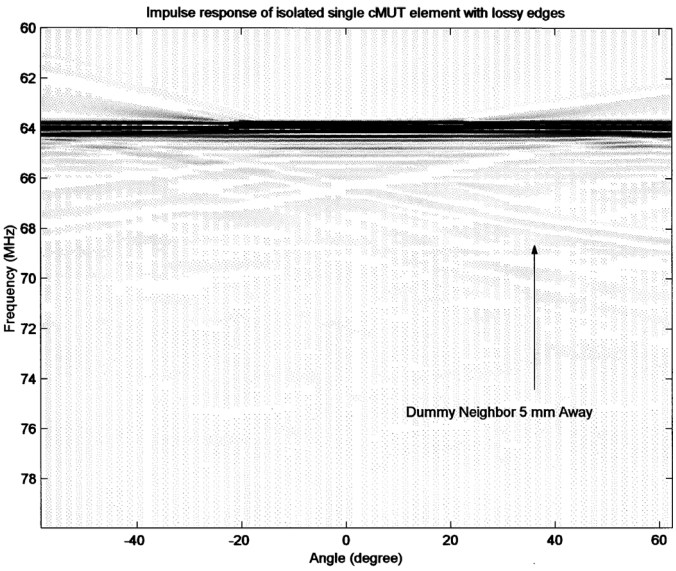

Fig. 22. Radiation pattern with silicon-soft, epoxy-liquid edges.

V. Conclusion

A 1-D cMUT array element is experimentally characterized, and the results are found to be in agreement with theoretical predictions. As a receiver, the transducer has a 0.28 fm/$\sqrt{Hz}$ displacement sensitivity, and, as a transmitter, it produces 5 kPa/V of output pressure at the transducer surface at 3 MHz. The transducer also has more than 100% fractional bandwidth around 3 MHz, which makes it suitable for ultrasound imaging.

The radiation pattern and crosstalk measurements on the array devices indicate that A0 mode Lamb wave in the substrate and Stoneley wave at the solid-liquid interface are important cross coupling sources. Several solutions to reduce the cross coupling have been suggested and tested. Further quantitative analysis has also been conducted, and it will be the subject of another paper.

The results reported herein indicate that cMUT arrays are an attractive alternative to piezoelectric array transducers in immersion ultrasonic imaging applications.

Acknowledgment

Special thanks are due to Dr. James P. McVittie, Tom Carver, Pauline Prather, and other technical staff in Ginzton Laboratory and Center for Integrated Systems of Stanford University. The optical displacement measurement instrument was provided by BMI.

References

[1] P. Eccardt, K. Niederer, and B. Fischer, "Micromachined transducers for ultrasound applications," in *Proc. Ultrason. Symp.*, 1997.

[2] I. Ladabaum, X. C. Jin, H. T. Soh, A. Atalar, and B. T. Khuri-Yakub, "Surface micromachined capacitive ultrasonic transducers," *IEEE Trans. Ultrason., Ferroelect., Freq. Contr.*, vol. 45, no. 3, pp. 678–690, May 1998.

[3] P. Eccardt, K. Niederer, T. Scheiter, and C. Hierold, "Surface micromachined ultrasound transducers in CMOS technology," in *Proc. Ultrason. Symp.*, pp. 959–962, 1996.

[4] X. C. Jin, I. Ladabaum, and B. T. Khuri-Yakub, "The microfabrication of capacitive ultrasonic transducers," *IEEE J. Microelectromech. Syst.*, vol. 7, no. 3, pp. 295–302, Sep. 1998.

[5] J. D. Larson, "Non-ideal radiators in phased array transducers," in *Proc. Ultrason. Symp.*, pp. 673–684, 1981.

[6] D. Certon, *et al.*, "Evaluation of laser probe performances for measuring cross coupling in 1-3 piezocomposite arrays," in *Proc. Ultrason. Symp.*, pp. 1091–1094, 1999.

[7] W. P. Mason, *Electromechanical Transducers and Wave Filters.* Van Nostrand, 1942.

[8] O. Oralkan, X. C. Jin, F. L. Degertekin, and B. T. Khuri-Yakub, "Simulation and experimental characterization of a 2-D capacitive micromachined ultrasonic transducer array element," *IEEE Trans. Ultrason., Ferroelect., Freq. Contr.*, vol. 46, no. 6, pp. 1337–1340, Nov. 1999.

[9] X. C. Jin, I. Ladabaum, F. L. Degertekin, S. Calmes, and B. T. Khuri-Yakub, "Fabrication and characterization of surface micromachined capacitive ultrasonic immersion transducers," *IEEE J. Microelectromech. Syst.*, vol. 8, no. 1, pp. 100–114, Mar. 1999.

[10] X. C. Jin, F. L. Degertekin, I. Ladabaum, S. Calmes, and B. T. Khuri-Yakub, "Micromachined capacitive transducer arrays for medical ultrasound imaging," in *Proc. Ultrason. Symp.*, pp. 1877–1880, 1998.

[11] I. A. Viktorov, *Rayleigh and Lamb Waves.* Plenum Press, 1967.

[12] G. S. Kino, *Acoustic Waves: Devices, Imaging, and Analog Signal Processing.* Prentice-Hall, Inc., 1987.

[13] B. A. Auld, *Acoustic Fields and Waves in Solids.* 2nd ed. R. E. Krieger, 1990.

[14] A. Atalar, "A fast method for calculating diffraction loss between two facing transducers," *IEEE Trans. Ultrason., Ferroelect., Freq. Contr.*, vol. 35, no. 5, pp. 612–617, Sept. 1988.

[15] F. L. Degertekin and B. T. Khuri-Yakub, "Single mode lamb wave excitation in thin plates by hertzian contacts," *Appl. Phys. Lett.*, vol. 69, no. 2, pp. 146–148, 1996.

[16] X. C. Jin, S. Calmes, C. H. Cheng, F. L. Degertekin, and B. T. Khuri-Yakub, "Micromachined capacitive ultrasonic immersion transducer array," in *Proc. Int. Conf. Solid-State Sens. Actuators*, pp. 1500–1503, 1999.

[17] H. Uberall, "Surface waves in acoustics," in *Physical Acoustics X.* W. Mason and R. Thurston, Eds. New York: Academic, 1973, pp. 1–60, ch. 1.

[18] F. Luppe and J. Doucet, "Experimental study of the stoneley wave at a plane liquid-solid interface," *J. Acoust. Soc. Amer.*, vol. 83, no. 4, pp. 1276–1279, Apr. 1988.

[19] W. P. Mason and R. N. Thurston, Eds., *Physical Acoustics: Principles and Methods.* vol. X, Academic Press, 1973.

Xuecheng Jin (S'95) received the BEng degree in biomedical engineering from Tsinghua University, PR China, in 1990 and the MEng degree in computer engineering from National University of Singapore, Singapore, in 1994. He is currently Senior Tutor at National University of Singapore and is studying toward a PhD degree in electrical engineering at Stanford University. His research interests include analog and mixed signal integrated circuits, micromachined sensors and actuators, and their applications in telecommunication and biomedicine. His industrial experiences are with Taixing Data Engineering Co, Texas Instruments, and Integrated Telecom Express Inc. He received Best Student Paper Awards in 1997 Ultrasonics International Conference and 1997 Meeting of the Acoustical Society of America and was the 1994 IEEE region 10 winner and 1998 IEEE region 3, 6, and 9 combined winner of the Student Paper Competitions in the IEEE Engineering in Medicine and Biology Society. He has more than 30 technical publications and 6 patents filed or granted. He is listed in the 18th edition of Who's Who in America. He is a member of IEEE.

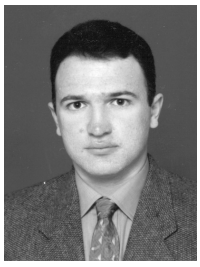

Ömer Oralkan (S'93) was born in Izmit, Turkey in 1973. He received the B.S. degree from Bilkent University, Ankara, Turkey, in 1995 and the M.S. degree from Clemson University, Clemson, SC, in 1997, both in electrical engineering. He is currently pursuing a Ph.D. degree in electrical engineering at Stanford University, Stanford, CA. From 1995 to 1996, he was a hardware and network engineer at Bilkent University Computer Center, Ankara, Turkey. In the summer of 1997, he worked as a process engineer at National Semiconductor Research Laboratories, Santa Clara, CA. His past and present research interests include analog and digital circuit design, micromachined sensors and actuators, and semiconductor device physics and fabrication. His current research focuses on front-end electronics design for 2-D capacitive micromachined ultrasonic transducer arrays for hand-held 3-D ultrasonic imaging systems. He is a member of IEEE.

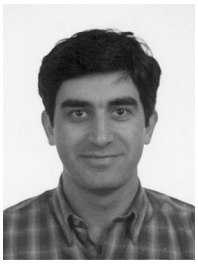

F. Levent Degertekin (M'90) was born in Diyarbakir, Turkey. He received the B.S. degree in 1989 from the Middle East Technical University, Turkey; the M.S. degree in 1991 from Bilkent University, Turkey; and the Ph.D. degree in 1997 from Stanford University, Stanford, CA, all in electrical engineering. He worked at the E. L. Ginzton Laboratory of Stanford University first as Visiting Scholar during the 1992-1993 academic year and then as Engineering Research Associate from 1997 to 2000. Currently, he is Assistant Professor in the MEMS research area at the G.W. Woodruff School of Mechanical Engineering of Georgia Institute of Technology, Atlanta, Georgia. His research interests include design and applications of micromachined ultrasonic transducers, micromachined sensors with integrated optoelectronic readout, and atomic force microscopy at ultrasonic frequencies.

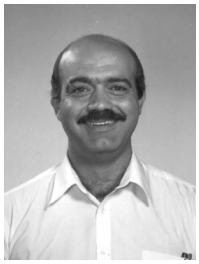

Butrus T. Khuri-Yakub (S'70–S'73–M'76–SM'87–F'95) was born in Beirut, Lebanon. He received the B.S. degree in 1970 from the American University of Beirut, the M.S. degree in 1972 from Dartmouth College, and the Ph.D. degree in 1975 from Stanford University, all in electrical engineering. He joined the research staff at the E. L. Ginzton Laboratory of Stanford University in 1976 as a research associate. He was promoted to Senior Research Associate in 1978 and to Professor of Electrical Engineering (Research) in 1982. He has served on many university committees such as graduate admissions, undergraduate academic council of the school of engineering, and others. He has been teaching both at the graduate and undergraduate levels for over 15 years, and his current research interests include in situ acoustic sensors (temperature, film thickness, resist cure, ...) for monitoring and control of integrated circuits manufacturing processes, micromachining silicon to make acoustic materials and devices such as air-borne and water immersion ultrasonic transducers and arrays, fluid ejectors, and the field of ultrasonic nondestructive evaluation and acoustic imaging and microscopy.

Professor Khuri-Yakub is a fellow of the IEEE, a senior member of the Acoustical Society of America, and a member of Tau Beta Pi. He is Associate Editor of *Research in Nondestructive Evaluation*, a journal of the American Society for Nondestructive Testing, and a member of the AdCom of the IEEE group on Ultrasonics Ferroelectrics, and Frequency Control (January 1994 to January 1997). He has authored over 300 publications and has been principal inventor or coinventor on over 50 patents. He received the Stanford University School of Engineering Distinguished Advisor Award (June 1987) and the Medal of the City of Bordeaux for contributions to NDE (1983).